

This is the accepted manuscript made available via CHORUS. The article has been published as:

Nature of Asymmetry in the Vibrational Line Shape of Single-Molecule Inelastic Electron Tunneling Spectroscopy with the STM

Chen Xu (✉), Chi-lun Chiang (✉), Zhumin Han (✉), and W. Ho

Phys. Rev. Lett. **116**, 166101 — Published 21 April 2016

DOI: [10.1103/PhysRevLett.116.166101](https://doi.org/10.1103/PhysRevLett.116.166101)

On the Nature of Asymmetry in the Vibrational Line Shape of Single-Molecule Inelastic Electron Tunneling Spectroscopy with the STM

Chen Xu,¹ Chi-lun Chiang,¹ Zhumin Han¹ and W. Ho^{1,2,*}

¹*Department of Physics and Astronomy, University of California, Irvine, California 92697-4575, USA*

²*Department of Chemistry, University of California, Irvine, California 92697-2025, USA*

PACS: 07.79.Fc, 68.43.Pq, 32.70.Jz, 33.70.Jg

Single molecule vibrational spectroscopy and microscopy has been demonstrated in 1998 by inelastic electron tunneling with the scanning tunneling microscope (STM). To date, the discussion of its application has mainly focused on the spatial resolution and the spectral energy and intensity. Here we report on the vibrational line shape for a single carbon monoxide molecule that qualitatively exhibits inversion symmetry when it is transferred from the surface to the tip. The dependence of the line shape on the molecule's asymmetric couplings in the tunnel junction can be understood from theoretical simulation and further validates the mechanisms of inelastic electron tunneling.

Inelastic electron tunneling spectroscopy (IETS) provides an excitation spectrum of vibrational modes by recording the small changes in the differential conductance as the voltage is ramped across the vibrational energy thresholds [1-4]. The combination of lock-in technology and stability of the tunneling gap in the scanning tunneling microscope (STM) enables IETS measurement of single molecules [4]. The vibrational energy is obtained from the peak position while the intensity is proportional to the vibrational excitation cross section [4, 5]. The line shape is more subtle and has not been resolved due to spectral broadening by the tip-sample temperature of the tunnel junction and amplitude of the lock-in modulation voltage [6-8]. However, the line shape contains information on the electron-vibration, the molecule-tip, and the molecule-substrate coupling strengths in the inelastic tunneling process [5, 9-11].

Vibrational IETS signatures of molecular junctions can appear as peaks [4, 12], dips [13, 14], and skewed features [15,16]. The origin of these various line shapes has been attributed to the interference between elastic and inelastic tunneling [11, 17-19]. However, the measured change in the differential conductance in IETS arises from the convolution of the elastic (negative change) and inelastic (positive change) channels that cannot be separated in the experiment. The onset of the inelastic channel influences the elastic channel and the measured change is the sum of the changes in both channels. Among all the theoretical efforts that have addressed the diverse line shapes observed in the vibrational IETS, the single channel model stands out for its simplicity and generality [5,9,10,17,20,21]. Within this model, the line shape in IETS can result from the correlation between the molecular resonance level in the tunnel junction and the molecule-tip (Γ_t) and molecule-substrate (Γ_s) couplings. But gating a single molecule

within the STM junction to shift the resonance level is a difficult task, and tuning Γ_t by changing the gap between the tip and adsorbed molecule does not produce significant changes in the IETS line shape because typically $\Gamma_t \ll \Gamma_s$ [22].

There is an extraordinary difference between Γ_s and Γ_t in the STM junction for molecules adsorbed on metal surfaces. Therefore, instead of tuning the tip-molecule tunneling gap or devising a gate electrode, the two opposing extremes ($\Gamma_s \gg \Gamma_t$ and $\Gamma_s \ll \Gamma_t$) can be realized in the STM by transferring the CO from the surface to the tip in a controlled manipulation. Furthermore, high energy resolution is required for resolving the line shape with a sub-Kelvin STM. The effects of the asymmetric tunnel junction on STM-IETS can therefore be determined, providing a deeper understanding of the line shape and the nature of inelastic tunneling.

The measurement by IETS was carried out with a home-built ultrahigh vacuum STM operated at ~ 600 mK and a base pressure of $\sim 5 \times 10^{-11}$ torr [23-25]. The Au(110) and Cu(100) surfaces and Ag tips were prepared by repeated cycles of sputtering and annealing. Dosing of CO molecules to achieve ~ 0.05 monolayer coverage on the Au(110) or Cu(100) surface was carried out at ~ 28 K. Under typical imaging conditions of 1 nA tunneling current and 10 mV sample bias, the topography of CO reveals adsorption on the atop site as a round protrusion on the Au(110) surface but a round depression on the Cu(100) surface. Spectra were normally recorded with the tip positioned over the center of these round depressions or protrusions. Tips were conditioned by occasional field emissions at ~ 5 V and repeated poking into the metal surface to produce sharp and stable tip configurations. Following these treatments, the apex of the Ag tip is coated by substrate atoms. This was verified by observing the vibrational spectrum for a CO

terminated tip measured over the bare Au(110) surface to be that of a CO adsorbed on the surface and measured by a metal tip [26]. Similarly, the Ag tip became coated with Cu atoms after poking into the Cu(100) surface, although we were not able to transfer CO from the Cu(100) surface to the tip.

There are four hindered vibrational modes for CO adsorbed on the atop site, besides the internal stretch and bouncing mode against the surface, as shown in Fig. 1a-d. For a surface with low symmetry, such as the Au(110) surface in Fig. 1e, the hindered translational mode (HT-mode) and the hindered rotational mode (HR-mode) have different energies. These two modes become degenerate when CO molecules are adsorbed on a high symmetry surface, such as the Cu(100) surface in Fig. 1f [12,27].

A STM-IETS spectrum for a single CO molecule adsorbed on Au(110) surface is shown in Fig. 2a and reveals both the HR-mode and the HT-mode. A splitting is found for the HR-modes due to the lifting of the degeneracy, with one peak at 30.8 meV (HR1 mode) and the other at 32.7 meV (HR2 mode). (The hindered translational (HT) mode is also split by ~ 0.8 meV and requires lower modulation bias voltage for its resolution.) The central features at ± 1 meV are associated with the zero bias differential conductance (dI/dV) dip (ZBCD). This dip in dI/dV is attributed to the effect of the Coulomb blockade or equivalently the reduction in current for low energy charged particles due to the space charge effect [28]. Furthermore, a difference is observed for the intensity of the HR-doublet. Most strikingly, the HR2 mode is more intense at positive bias, but the HR1 mode is more intense at negative bias. In contrast, it is expected for a symmetric junction that the molecular vibration would be similarly excited for electrons tunneling from the tip (positive bias) or from the substrate (negative bias) so that the relative intensity of the

two HR modes should be independent of the bias polarity. The dependence of the relative intensity on the bias polarity has its origin in the asymmetry of the tunneling junction.

The vibrational spectrum by STM-IETS with the CO-terminated tip positioned over a surface Au atom is shown in Fig. 2b, revealing the CO vibrational excitations at 3.9 meV (HT-mode) and 31.3 meV (HR-mode). The modes are present at all positions of the surface and close in energies as those for CO adsorbed on top of an Au atom (atop site) of the Au(110) surface (Fig. 2a), confirming that the tip is coated with Au atoms and terminated with a CO molecule. The two HR-modes are not split, suggesting that the CO is adsorbed in a high symmetry site of the tip [29]. Furthermore, the line shape of the HR-mode is not symmetric with falling tail at left side and a shallow dip at right side of the peak at positive bias, but with rising tail at the left side and a shallow peak at the right side of the dip at negative bias. This asymmetry could explain the different intensity of the HR-doublet for CO on the Au(110) surface (Fig. 2a) as resulting from the sum of two asymmetric line shapes of similar intensity in the doublet.

The schematic in Fig. 2c and 2d show that CO is coupled with different strengths to the substrate and the tip, depending on the side of the junction to which it is adsorbed. When CO is adsorbed on the surface, the rates yield $\Gamma_t < \Gamma_s$, as shown in Fig. 2c. The coupling of the CO to the tip is strengthened ($\Gamma_t > \Gamma_s$) when it is transferred from the surface to the tip, as shown schematically in Fig. 2d. The resolution in the topographic image is enhanced with a CO-terminated tip, as are displayed for a bare (Fig. 2e) and a CO-terminated tip (Fig. 2f). The observation of atomic resolution for the substrate surface indicates a functionalized tip, in addition to the vibrational signatures of CO by IETS.

The understanding of asymmetry in the STM-IETS line shape can be further validated by analyzing CO molecules adsorbed on four-fold symmetric Cu(100) surface with a Cu-coated Ag tip, as shown in Fig. 3a and Fig. 3b. Both the HT-doublet and the HR-doublet of CO become degenerate and are detected at 4.1 meV and 35.1 meV, respectively, as shown by the IETS spectrum in Fig. 3c. The line shape for the HR-mode is notably asymmetric. Since the CO molecule couples more strongly to the substrate than to the tip ($\Gamma_s \gg \Gamma_t$), the asymmetry in the line shape of the HR-mode is on the opposite side of the peak at positive bias compared to that with CO on the tip in Fig. 2b (and similarly for the dip at negative bias.)

The asymmetry in the line shape can be explained by simulation using the single channel model [9,10,20]. Based on the non-equilibrium Green's function formalism and the approximation by the lowest order expansion, the tunneling current can be divided into a Landauer term and two universal function terms I^{sym} and I^{asym} , where dI^{sym}/dV is an even function of the bias and dI^{asym}/dV is an odd function of the bias. The Landauer term describes the trivial linear dependency of tunneling current on bias and its second derivative is zero. The dI^{asym}/dV term depends on the balance between Γ_s and Γ_t ; it completely vanishes when $\Gamma_s = \Gamma_t$. The asymmetry in the line shape changes from one side to the other of the d^2I/dV^2 peak or dip, as shown in Fig. 4a and Fig. 4b for $\Gamma_s \gg \Gamma_t$ and $\Gamma_s \ll \Gamma_t$. The parameters are chosen such that the closest resonance lies away from the Fermi surface (off-resonance case) [22]. Detail of the simulation can be found in the supplemental material [30]. As illustrated in Fig. 4, the STM-IETS spectrum is the addition of d^2I^{sym}/dV^2 and d^2I^{asym}/dV^2 , where d^2I^{sym}/dV^2 yields the outline of the spectrum while d^2I^{asym}/dV^2 produces the small asymmetric correction. With the couplings changes

from $\Gamma_s \gg \Gamma_t$ to $\Gamma_t \gg \Gamma_s$, the outline of IETS stays the same while the small asymmetric correction changes in sign:

$$\frac{d^2 I^{sym}(\Gamma_t, \Gamma_s)}{dV^2} = \frac{d^2 I^{sym}(\Gamma_s, \Gamma_t)}{dV^2}$$

$$\frac{d^2 I^{asym}(\Gamma_t, \Gamma_s)}{dV^2} = -\frac{d^2 I^{asym}(\Gamma_s, \Gamma_t)}{dV^2}$$

Therefore, the asymmetry in the IETS line shape changes as Γ_s and Γ_t reverse in strength.

The simulation of the doublet in the IETS spectrum for CO adsorbed on Au(110), a surface of lower symmetry (Fig. 4c), provides an explanation to the observed relative intensity of the two peaks at positive and negative biases. It should be noted that in the simulation, the exact values of Γ_s and Γ_t are chose arbitrarily and only their relative strengths can be experimentally deduced.

We are also able to observe similar line shape asymmetry for CO on the Cu(111) surface (not shown here). It should also be noted that the asymmetry in the line shape is less prominent for the Ag(110) surface (see Fig.1B and 1D in Ref. [25]). This reduced asymmetry is attributed to $\Gamma_s \approx \Gamma_t$, because CO-Ag coupling is weaker than CO-Au coupling or CO-Cu coupling. This is corroborated by the relative energy of the HR-mode, which is lowest for CO-Ag (~20 meV) compared to CO-Au (~30 meV) and CO-Cu (~35 meV). This trend in energy also holds for the HT-mode. The weak CO-Ag coupling has also been confirmed by theoretical calculations [31].

In a previous work of A. J. Heinrich et al., a similar line shape asymmetry can also be observed in the IETS spectrum for a bare tip probing a CO $\sqrt{3} \times \sqrt{3}$ array adsorbed on the Cu(111) surface (see Fig. 4A and Fig. 6B in Ref. [32]). This asymmetry changes when the bare tip was positioned over a chevron-shaped CO assembly. Based on

the single channel model, the reason for such a change may be attributed to variation of the adsorbate resonance level. However, the exact mechanism calls for theoretical investigation.

In summary, we report the existence of vibrational asymmetry in the off-resonance STM-IETS that can only be resolved with high energy resolution at below 1 K. Such measurements reveal that the line shape asymmetry results from the difference in strength between the molecule-tip coupling Γ_t and the molecule-substrate coupling Γ_s . Based on the non-equilibrium Green's function formalism and the approximation of the lowest order expansion, the single channel model was adopted to simulate the line shape of the IETS spectra, and a consistent agreement between experiment and theory has been achieved. The confirmation of the spectral asymmetry in STM-IETS provides a deeper understanding into the mechanisms of vibrationally inelastic electron tunneling.

ACKNOWLEDGMENTS

We have benefited from stimulating discussions with M. Paulsson, H. Ueba, M. Persson, and S. Li. This work was mainly supported by the Chemical Sciences, Geo- and Bioscience Division, Office of Science, U.S. Department of Energy, under grant DE-FG02-04ER15595 (CX), DE-FG02-06ER15826 (ZH), and additionally by the Condensed Matter Physics Program, Division of Materials Research, National Science Foundation, under grant DMR-1411338 (CJ).

* To whom correspondence should be addressed.

wilsonho@uci.edu

References and Notes

- [1] R.C. Jaklevic and J. Lambe, Phys. Rev. Lett. **17**, 1139 (1966).
- [2] G. Binnig, N. Garcia, and H. Rohrer, Phys. Rev. B **32**, 1336 (1985).
- [3] B. N. J. Persson and A. Baratoff, Phys. Rev. Lett. **59**, 339 (1987).
- [4] B. C. Stipe, M. A. Rezaei, and W. Ho, Science **280**, 1732 (1998).
- [5] A. Baratoff and B. N. J. Persson, J. Vac. Sci. Technol. A **6**, 331 (1988).
- [6] L. J. Lauhon and W. Ho, Rev. Sci. Instrum. **72**, 216 (2001).
- [7] S. Paavilainen and M. Persson, Phys. Rev. B **74**, 085417 (2006).
- [8] S. Monturet, M. Alducin, and N. Lorente, Phys. Rev. B **82**, 085447 (2010).
- [9] M. Paulsson, T. Frederiksen, and M. Brandbyge, Phys. Rev. B **72**, 201101 (2005).
- [10] M. Paulsson, T. Frederiksen, and M. Brandbyge, J. Phys.: Conference Series **35**, 247 (2006).
- [11] M. Galperin, M. A. Ratner, and A. Nitzan, J. Chem. Phys. **121**, 11965 (2004).
- [12] L. J. Lauhon and W. Ho, Phys. Rev. B **60**, R8525 (1999).
- [13] J. R. Hahn, H. J. Lee, and W. Ho, Phys. Rev. Lett. **85**, 1914 (2000).
- [14] R. H. M. Smit, Y. Noat, C. Untiedt, N. D. Lang, M. C. van Hemert, and J. M. van Ruitenbeek, Nature **419**, 906 (2002).
- [15] W. Y. Wang, T. Lee, I. Kretzschmar, and M. A. Reed, Nano Lett. **4**, 643 (2004).
- [16] S. Li, A. Yu, F. Toledo, Z. Han, H. Wang, H.Y. He, R. Wu, and W. Ho, Phys. Rev. Lett. **111**, 146102 (2013).
- [17] H. Ueba, T. Mii, and S. G. Tikhodeev, Surf. Sci. **601**, 5220 (2007).
- [18] N. Lorente and M. Persson, Phys. Rev. Lett. **85**, 2997 (2000).
- [19] M. Persson, Phil. Trans. R. Soc. A **362**, 1173 (2004).
- [20] M. Paulsson, T. Frederiksen, H. Ueba, N. Lorente, and M. Brandbyge, Phys. Rev. Lett. **100**, 226604 (2008).
- [21] M. Galperin, M. Ratner, and A. Nitzan, Nano Lett. **4**, 1605 (2004).
- [22] L. Vitali, R. Ohmann, K. Kern, A. Garcia-Lekue, T. Frederiksen, D. Sanchez-Portal, and A. Arnau, Nano Lett. **10**, 657 (2010).
- [23] U. Ham and W. Ho, Physical Rev. Lett. **108**, 106803 (2012).

- [24] U. Ham and W. Ho, J. Chem. Phys. **138**, 074703 (2013).
- [25] C.L. Chiang, C. Xu, Z. Han, and W. Ho, Science **344**, 885 (2014).
- [26] Here the spectrum is not exactly the same as that for CO on Au(110), but it is definitely not the spectrum for CO on Ag surface, where the hindered rotational mode is around 20 meV.
- [27] J. Ahner, D. Mocuta, R. D. Ramsier, and J. T. Yates, Jr., Phys. Rev. Lett. **79**, 1889 (1997).
- [28] R. Egerton, Reports on Progress in Physics **72**, 016502 (2008).
- [29] It is possible that the apex of the Au (or Cu) coated Ag tip may possess an anisotropy. The splitting due to that anisotropy, if present, would be smaller than our energy resolution of ~ 0.8 meV since it is not resolved in the spectra. It is also possible that CO is not attached to the tip apex. Before taking any IETS spectrum, however, we made sure that the CO-tip is symmetric by scanning over another CO adsorbed on the surface. The topographic image is very sensitive to the CO-tip, and only those CO-tips showing symmetrically circular topographic image of an adsorbed CO are used for recording the IETS spectra. Additionally, if the CO is not adsorbed at the tip apex, the IETS spectrum would show weak or no vibrational features.
- [30] See the supplementary material for details, the code is also available at <https://github.com/iets-lineshape/simulation>
- [31] N. Lorente and H. Ueba, The European Physical Journal D **35**, 341 (2005).
- [32] A. J. Heinrich, C. Lutz, J. Gupta, and D. Eigler, Science **298**, 1381 (2002).

Figure Captions

FIG. 1. Adsorption of CO on surfaces with different symmetry. (a-d) Schematic diagrams showing the six vibrational modes of CO adsorbed on metal surfaces (the corresponding motions perpendicular to the plane of the paper for the hindered rotational (HR) mode in (c) and hindered translational (HT) mode in (d) are not shown.) Top view of (e) Au(110) and (f) Cu(100) surfaces with an isolated CO molecule adsorbed on top of a surface atom. The surface anisotropy of Au(110) lifts the degeneracy of the HT-mode and the HR-mode which are doubly degenerate on the Cu(100) surface.

FIG. 2. The asymmetric tunneling gap with CO adsorbed on two-fold symmetric Au(110) surface and to the tip. (a) Vibrational STM-IETS d^2I/dV^2 spectrum taken with Au coated tip for single CO adsorbed on the atop site of the row of atoms. The upper curve (blue) is recorded over a CO molecule; the lower curve (red) is over a row of the Au(110) surface (spectrum is similar over the trough between two rows). Bias modulation: 1 mV at 471 Hz, and tunneling gap set point: $V = 20$ mV and $I = 1$ nA. The doublet for the HR-mode at 30.8 meV and 32.7 meV shows reversed relative peak intensities for opposite bias polarities due to asymmetry in the line shape. The green curve in the inset is for the doublet of the HT-mode at 4.1 meV and 4.9 meV, taken with modulation 300 μ V at 471 Hz and tunneling gap set point: $V = 10$ mV and $I = 1$ nA. The line shape of the HT-mode is obscured by the zero bias conductance dip (ZBCD) at 1 meV (as shown isolated in the spectrum taken over the Au surface.) (b) STM-IETS with CO-terminated tip measured over the Au(110) surface. Bias modulation: 1 mV at 471 Hz, and tunneling gap set point: $V = 10$ mV and $I = 1$ nA. The energy of the HR-mode at 31.3 meV is the same as the

average of the doublet for a Au-coated tip over a CO on the Au surface, indicating that the tip is coated with Au atoms. The line shape for the HR-mode is asymmetric, but is obscured by the ZBCD for the HT-mode. Schematic diagrams of the geometric configurations for (c) the metal tip probing single CO on Au(110) surface and (d) the CO-terminated tip probing Au(110) surface. (e) STM topography of CO adsorbed on Au(110) surface ($20 \text{ \AA} \times 20 \text{ \AA}$), taken with a metal tip. Set point: $V = 10 \text{ mV}$ and $I = 1 \text{ nA}$. (f) STM topography of CO-terminated tip probing the Au(110) surface ($20 \text{ \AA} \times 20 \text{ \AA}$). Set point: $V = 2 \text{ mV}$ and $I = 1 \text{ nA}$. Surface atoms are resolved. The palette in e and f shows the relative topographic variation in Ångström unit by defining the lowest tunneling gap as 0 \AA .

FIG. 3. Adsorption of CO on four-fold symmetric Cu(100) probed with a metal tip. (a) Schematic diagram of the tunneling gap configuration. (b) STM topographic image of CO ($20 \text{ \AA} \times 20 \text{ \AA}$). Tunneling gap set point: $V = 4 \text{ mV}$ and $I = 4 \text{ nA}$. The palette in e and f shows the relative topographic variation in Ångström unit by defining the lowest tunneling gap as 0 \AA . (c) STM-IETS over CO (lower spectrum in blue). ZBCD is observed over the substrate (upper spectrum in red). Bias modulation: 1 mV at 471 Hz , and tunneling gap set point: $V = 20 \text{ mV}$ and $I = 1 \text{ nA}$.

FIG. 4. Simulation of STM-IETS using the single channel model from Ref. 20. Refer to the online supplemental materials for more details. Simulation of CO on Cu(100): (a) $\Gamma_s \gg \Gamma_t$, and (b) $\Gamma_t \gg \Gamma_s$. The red dashed curve is $d^2 I^{\text{sym}}/dV^2$ and the black dotted curve is $d^2 I^{\text{asym}}/dV^2$. The $d^2 I^{\text{sym}}/dV^2$ remains the same and $d^2 I^{\text{asym}}/dV^2$ changes sign when Γ_s and Γ_t

are reversed in relative strength. The sum of d^2I^{sym}/dV^2 and d^2I^{asym}/dV^2 is shown as the solid curve in blue. (c) and (d) Simulation of the doublet for the HR mode in STM-IETS for metal tip probing CO adsorbed on Au(110) surface. The red and black curves represent individual spectrum by IETS for the two HR modes, taken to be equal intensity, with the sum of the two spectra shown by the blue curve. The asymmetry in the line shape for each HR mode leads to the overall asymmetry of the sum.

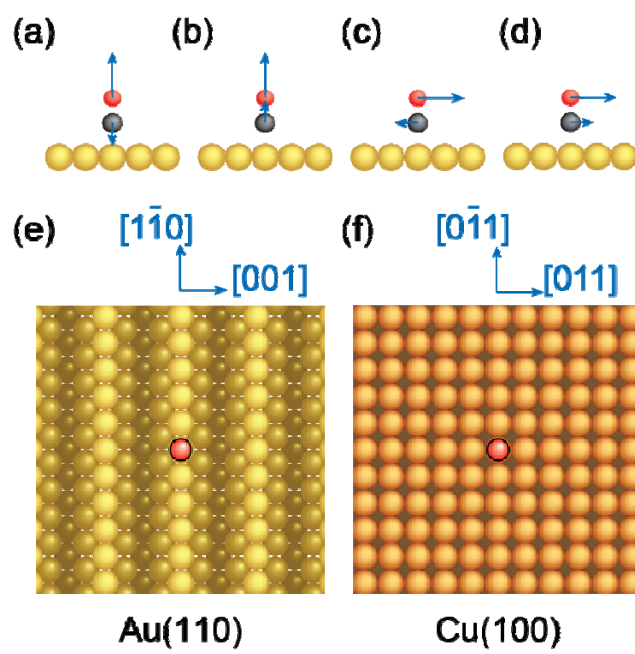


Figure 1

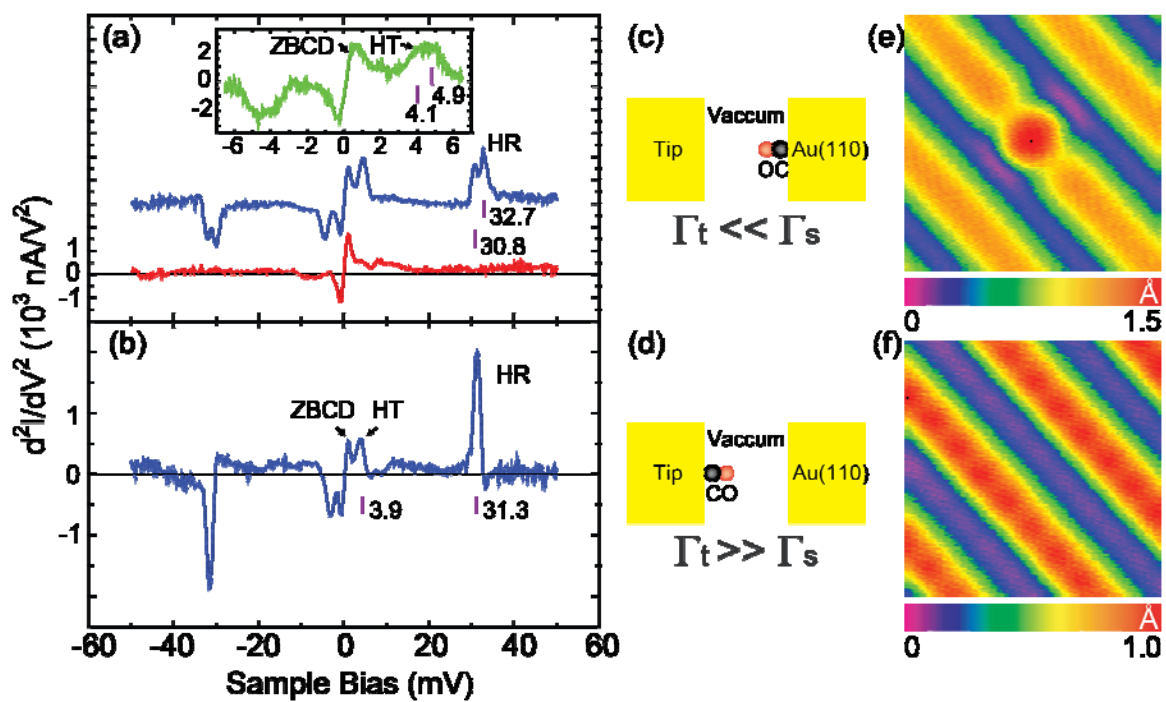


Figure 2

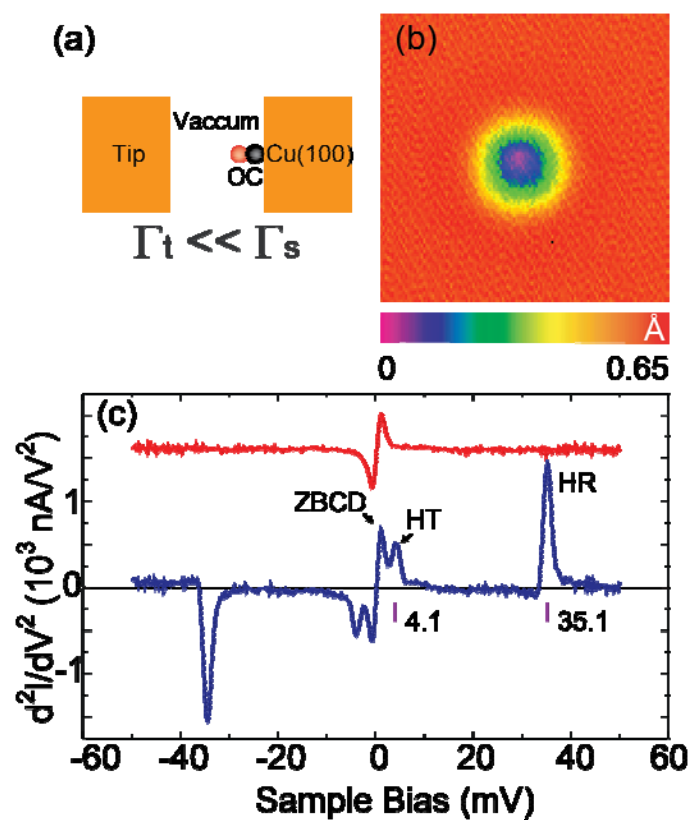


Figure 3

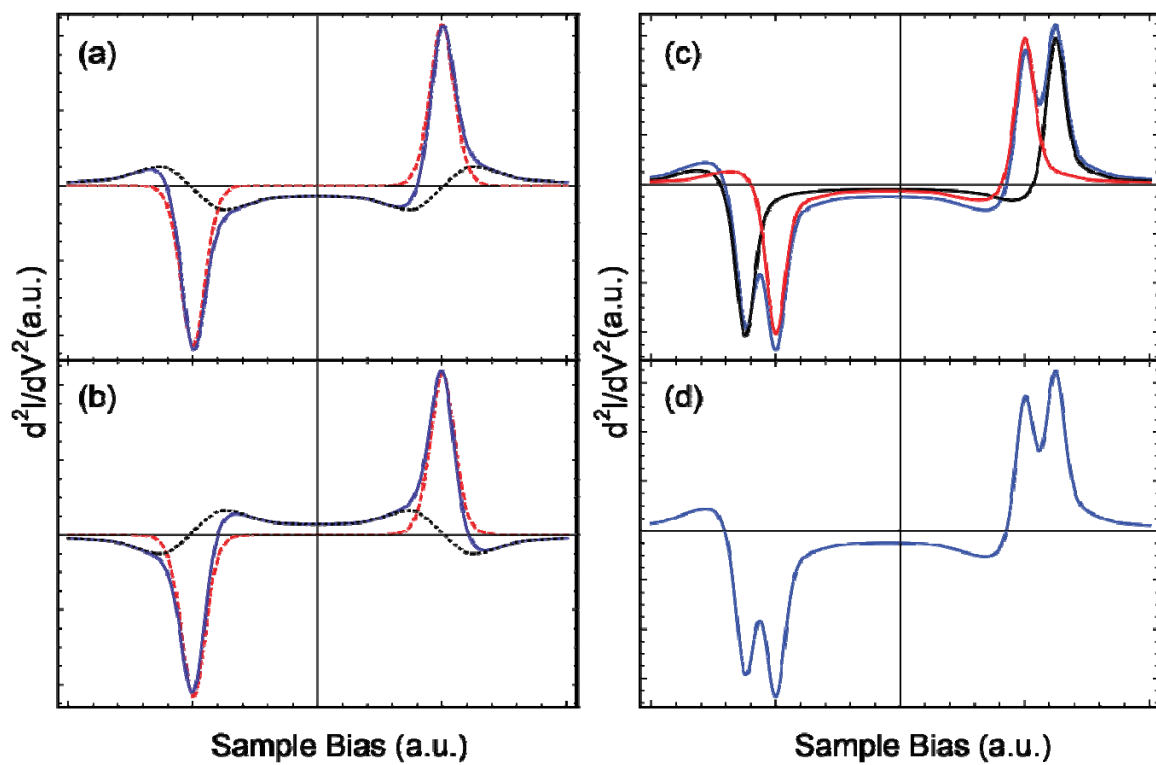


Figure 4